



# Prevention of well clogging during aquifer storage of turbid tile drainage water rich in dissolved organic carbon and nutrients

Emiel Kruisdijk<sup>1,2</sup> · Julian F. Ros<sup>1</sup> · Devanita Ghosh<sup>1</sup> · Maren Brehme<sup>1</sup> · Pieter J. Stuyfzand<sup>1,3</sup> · Boris M. van Breukelen<sup>1</sup>

Received: 25 April 2022 / Accepted: 19 January 2023 / Published online: 9 February 2023  
© The Author(s) 2023

## Abstract

Well clogging was studied at an aquifer storage transfer and recovery (ASTR) site used to secure freshwater supply for a flower bulb farm. Tile drainage water (TDW) was collected from a 10-ha parcel, stored in a sandy brackish coastal aquifer via well injection in wet periods, and reused during dry periods. This ASTR application has been susceptible to clogging, as the TDW composition largely exceeded most clogging mitigation guidelines. TDW pretreatment by sand filtration did not cause substantial clogging at a smaller ASR site (2 ha) at the same farm. In the current (10 ha) system, sand filtration was substituted by 40- $\mu\text{m}$  disc filters to lower costs (by 10,000–30,000 Euro) and reduce space (by 50–100 m<sup>2</sup>). This measure treated TDW insufficiently and injection wells rapidly clogged. Chemical, biological, and physical clogging occurred, as observed from elemental, organic carbon, 16S rRNA, and grain-size distribution analyses of the clogging material. Physical clogging by particles was the main cause, based on the strong relation between injected turbidity load and normalized well injectivity. Periodical backflushing of injection wells improved operation, although the disc filters clogged when the turbidity increased (up to 165 NTU) during a severe rainfall event (44 mm in 3 days). Automated periodical backflushing, together with regulating the maximum turbidity (<20 NTU) of the TDW, protected ASTR operation, but reduced the injected TDW volume by ~20–25%. The studied clogging-prevention measures collectively are only viable as an alternative for sand filtration when the injected volume remains sufficient to secure the farmer's needs for irrigation.

**Keywords** Artificial recharge · Managed aquifer recharge (MAR) · Well clogging · Agriculture

## Introduction

Managed aquifer recharge (MAR) is becoming an important technique for water management in response to increasing water scarcity and global climate change (Dillon et al. 2019; Greve et al. 2018; Stikker 1998). Excess water is stored in an aquifer during wet periods and later abstracted to overcome water shortages during dry

periods. The technique provides storage with a minimal use of above-ground space and prevents the loss of water by evaporation (Page et al. 2018; Pyne 1995). Aquifer storage transfer and recovery (ASTR) is one of the methods allowing for excess water to be stored in an aquifer. It comprises injection wells and a recovery system composed of abstraction wells, utilizing the aquifer to improve water quality via physical and biogeochemical processes during subsurface transport (Dillon 2005; Pyne 1995). Aquifer storage and recovery (ASR), as opposed to ASTR, utilizes a single well for injection and abstraction.

A major drawback of AS(T)R is the risk of well clogging. Injection wells are more prone to clogging compared to abstraction wells, especially when source water quality is poor (Page et al. 2018). Dillon et al. (1994) surveyed 40 ASR sites in the United States and concluded that about 80% of injection wells suffered from clogging. Clogging results in a reduction of the injection rate, which threatens AS(T)R feasibility (Maliva 2020). This can occur within minutes to

✉ Emiel Kruisdijk  
e.kruisdijk@tudelft.nl

<sup>1</sup> Department of Water Management, Faculty of Civil Engineering and Geosciences, Delft University of Technology, Stevinweg 1, 2628 CN Delft, The Netherlands

<sup>2</sup> Acacia Water B.V, Van Hogendorpplein 4, 2805 BM Gouda, The Netherlands

<sup>3</sup> Stuyfzand Hydroconsult+, 2042 BL Zandvoort, The Netherlands

weeks of AS(T)R operation (Olsthoorn 1982; Rinck-Pfeiffer et al. 2000), after which well rehabilitation is necessary to restore injection rates (Jeong et al. 2018; Martin 2013).

Physical, biological, chemical, and mechanical processes induce injection-well clogging (Martin 2013). Olsthoorn (1982) and Pyne (1995) laid a strong scientific foundation on clogging, and concluded that physical and biological processes often dominate. Particles in injected water can cause physical clogging. Martin (2013) and Pyne (1995) stated for that reason that turbidity levels should be reduced to 1–5 nephelometric turbidity units (NTU) to reduce physical clogging. Furthermore, column studies showed that injection water should contain suspended solids below 2 mg/L to sustain injection rates (Okubo and Matsumoto 1983), while concentrations as low as 0.1 mg/L are recommended in practice (Zuurbier and van Dooren 2019). Biological clogging results from microbial growth. Injection rates can substantially be reduced by growing biofilms of impermeable slime and mats of (dead) cells (Pyne 1995). Biological clogging can be reduced by taking away the substrates needed for microbial metabolism from injected water, for example, by reducing dissolved organic carbon (DOC) concentrations below 2 mg/L (Zuurbier and van Dooren 2019), ammonium concentrations below 0.5 mg/L (Hubbs 2006), and eliminating high concentrations of nitrate and phosphate (Eom et al. 2020; Stuyfzand and Osma 2019).

The other two clogging mechanisms are chemical and mechanical clogging. Chemical clogging occurs due to the precipitation of carbonates, Fe- and Mn-(hydr)oxides, and other minerals (Martin 2013). Mineral precipitation is often mediated by microorganisms, which makes it difficult to distinguish chemical from biological mechanisms (Martin 2013; Rinck-Pfeiffer et al. 2000). Mechanical clogging is caused by injecting entrained air, or by the production of biogenic gases within the aquifer by microbial activity (Martin 2013).

Treatment of the water before injection can prevent these clogging mechanisms. For example, (1) Page et al. (2011) injected high-nutrient and high-turbidity storm water after treatment by ultrafiltration and granular activated carbon and did not observe major clogging; (2) Camprovin et al. (2017) showed that injection of sand-filtered surface water in a coarse sandy aquifer can substitute the injection of potable water, although some clogging was detectable. Nevertheless, the options for treatment are often limited because of financial and spatial constraints.

In this study, an agricultural ASTR system was studied in which tile drainage water (TDW) from an agricultural parcel (10 ha) was collected, injected in an aquifer, and recovered when needed for crop irrigation. TDW composition exceeded most of the clogging mitigation guidelines (e.g., mean injected DOC: 25 mg/L,  $\text{NO}_3^-$ : 14 mg/L, turbidity: 2–165 NTU) and, therefore, the injection wells were

susceptible to clogging. The system studied in the current research replaced a successful smaller-scale agricultural ASR system (2.3 ha) equipped with a sedimentation basin and slow and rapid sand filtration as clogging-prevention measures (Tolk and Veldstra 2016). This system did not clog substantially during the injection of  $\sim 27,000 \text{ m}^3$  tile drainage water (TDW) over more than 3 years. The new system was designed to occupy a smaller surface area, while reducing the costs of treatment. The slow and rapid sand filtration and sedimentation basin were therefore substituted with disc filters, which resulted in an estimated spatial gain of about 50–100  $\text{m}^2$  and a reduction of 10,000–30,000 Euro on building costs (costs and space extrapolated from the prior ASR site, based on quotations). Obtained insights are not only useful for the specific region studied in this research, but for any other similar system when built, as similar exceedances of the clogging mitigation guidelines are expected. Implementation of agricultural AS(T)R for freshwater availability has potential worldwide, as agricultural fields with tile drainage are common. For example, about 17% of cropland in the USA (Pavelis 1987) and 34% in Northwest Europe (Abbott and Leeds-Harrison 1998) have been altered by artificial surface or subsurface drainage, and Smedema and Ochs (1997) estimated that drainage systems are used in one-third of the land area where natural drainage constrains agricultural development and/or production.

Well clogging was assessed during ASTR where TDW was treated using disc filters. Subsequently, automated periodic backflushing of the injection wells was added to the system, followed by the addition of automated turbidity regulation to prevent the injection of turbid TDW. These latter two measures are also relatively low cost and do not claim additional space. The three set-ups with an increasing number (1, 2, and 3) of clogging prevention measures were monitored during three injection periods over 1.5 years. This study evaluated the clogging potential of TDW at the ASTR site during these periods by monitoring the normalized well injectivity, the turbidity of TDW before and after treatment, and the interior of the wells using a camera. Furthermore, the main clogging mechanisms were diagnosed by elemental, organic carbon, 16S rRNA, and grain-size-distribution analysis of the clogging material.

## Materials and Methods

### Description of the ASTR system

The research site is located in a coastal polder close to the town of Breezand, in the province of North Holland, the Netherlands—coordinates (decimal degrees): 52.8883, 4.8221; (Fig. 1). In this area, tile drainage commonly prevents water damage to crops (flower bulbs at this research

site) by quickly discharging water to the surface-water system during and after rainfall events. The drains are situated in a shell bed at approximately 70 cm-below surface level (bsl) in a 1-m sandy layer above a confining clay layer. In the current system, tile drainage water (TDW) does not enter the surface-water system, but rather is distributed to a drain reservoir (volume =  $\sim 1 \text{ m}^3$ ). In this reservoir, TDW is continuously sensed on electrical conductivity (EC) as a measure of salinity. TDW with an  $\text{EC} > 1,700 \text{ }\mu\text{S/cm}$  is directly discharged to the surface-water system. The remaining sufficiently fresh TDW is stored in the brackish/saline aquifer below the confining clay layer by an ASTR system. First, water is pumped from the reservoir and filtered by seven 40- $\mu\text{m}$ -2" Spin Klin disc filters (Netafim, Israel) in series—Fig. S2 of the electronic supplementary material (ESM). The pump in the drain reservoir ensures the required pressure for disc filter operation and a constant 3-m standing head in the standpipe which is required for injection. To prevent clogging, every disc filter was backflushed for 20 s. Backflushing was initiated once the differential pressure over the filters exceeded 0.6 bar; additionally, the filters were backflushed every 6 h. TDW, used for backflushing of the filters, was discharged to the surface-water system; afterwards, it was injected into the aquifer via two injection wells. In times of drought, stored TDW can be abstracted by four abstraction wells surrounding the injection wells at about 7 m distance, and reused for irrigation. A more detailed schematic representation of the ASTR system can be found in section S1 of the ESM.

Injection occurred in about equal proportions through injection wells one (INJ-1) and two (INJ-2) (well screens from 11.5 to 33 m bsl). The maximum injection capacity is approximately  $14 \text{ m}^3/\text{h}$  per well. INJ-1 and INJ-2 are situated 5 m apart (PVC, borehole diameter = 240 mm, internal well diameter = 100 mm, slot size = 0.5 mm). A monitoring well (MW) is fixed at the midpoint of the gravel pack (approximately 35 mm from the well screen) screened at 20.5 to 22.5 m bsl (internal diameter = 25.4 mm, slot size = 0.5 mm) at both injection wells. MW-1 and MW-2 correspond to the monitoring wells in the gravel pack of INJ-1 and INJ-2, respectively.

Four abstraction wells (ABS-1 to ABS-4) surround INJ-1 and INJ-2 in a symmetrical configuration (Fig. 1). The abstraction wells are screened from 12 to 23 m bsl (borehole diameter = 400 mm, internal well diameter = 190 mm, slot size = 0.5 mm). Each borehole contains a MW in the gravel pack approximately 50 mm from the well screen, screening a depth of 16.5–18.5 m bsl (PVC, internal diameter = 24.5 mm, slot size = 0.5 mm). MW-3 to MW-6 correspond to the monitoring well situated in the borehole of ABS-1 to ABS-4, respectively.

The Dutch national database DINOloket (GeoTOP v1.4 model) provided insights regarding the large-scale

hydrogeological structure of the target aquifer (TNO-NITG, TNO-NITG DINOloket 2021). The agricultural topsoil is an approximately 1-m coarse sand layer in which the tile drains are situated, while below, there is a confining layer of  $\sim 10 \text{ m}$  thickness consisting mostly of clay and peat. The ASTR target aquifer is found below the confining layer ranging to about 40 m bsl, consisting mostly of unconsolidated fine-to-coarse sand of Holocene and Pleistocene age. The groundwater level in the target aquifer is about 1 m bsl. The electrical conductivity increases from about  $1,900 \text{ }\mu\text{S/cm}$  at 12 m bsl to more than  $9,000 \text{ }\mu\text{S/cm}$  at 32 m bsl.

## Set-up of the ASTR clogging study

### ASTR operation

Three periods of injection were monitored between October 2019 and March 2021, during which time approximately  $5,000 \text{ m}^3$  TDW was injected in each of the injection wells. In the first period,  $1,350 \text{ m}^3$  TDW was injected per well from 31 October 2019 until 12 December 2019. Well clogging occurred during this period. Afterwards, an automated backflush system was installed in both INJ-1 and INJ-2, to prevent rapid clogging of these wells. The automated regime consisted of a 15-min backflush of  $20 \text{ m}^3/\text{h}$  in each well, which occurred after consecutive injection of  $150 \text{ m}^3$  per well. The injected volume was reduced to  $50 \text{ m}^3$  after 2 weeks of operation, as indications of clogging were still observed. In this period,  $1,450 \text{ m}^3$  TDW was injected per well from 20 September 2020 until 16 October 2020. In the third period, a turbidity sensor was installed in the drain reservoir to further diminish clogging. The monitored turbidity was used for the regulation of ASTR operation.  $\text{TDW} > 20 \text{ NTU}$  was directly discharged to the surface-water system to prevent clogging of the disc filters and injection wells. During this period,  $2,150 \text{ m}^3$  was injected per well from 8 December 2020 until 18 March 2021. Stored water was not yet abstracted by the abstraction wells during the period of investigation at this ASTR pilot, only for backflushing and sampling.

Phreatic groundwater levels rise quickly in the agricultural topsoil during and after large rainfall events. This can result in crop damage and, therefore, quick drainage of TDW is needed. The injection capacity of the ASTR system was not adequate to drain all TDW from the field during large rainfall events. Therefore, TDW was discharged to the surface-water system during these events in the first injection period. In the second and third injection periods, the system was adapted so that TDW could be partly discharged to the surface-water system and partly injected via the injection wells. As a result, a part of the water could be stored during these events, because the same pump was used simultaneously for the discharge to the surface-water system and to

the injection wells. However, less water entered the ASTR system, which resulted in a lower standing head in the standpipe and a reduced injection capacity.

### Clogging monitoring

Clogging of INJ-1 and INJ-2 was examined by continuous monitoring (10-min interval) of water pressure in MW-1, MW-2, and MW-3 using CTD divers (van Essen Instruments, the Netherlands). Barometric pressure was measured using a baro-diver (van Essen Instruments, the Netherlands). Unfortunately, the barometric pressure data could not be obtained from the baro-diver between February 7 and March 18, 2021 (third injection period). Instead, daily barometric pressures were obtained from the local weather station de Kooy, Den Helder (about 5 km from the research site). This resulted in a lower resolution of calculated phreatic surface levels, injectivity index, and the hydraulic head rise in the third injection period.

Injected volumes and injection rates were continuously monitored during the second and third periods with Arad Octave ultrasonic water meters. A relation was obtained between the injection rate ( $\text{m}^3/\text{h}$ ) and the head rise in MW-3 (cm) for the second and third periods (Eq. 1,  $R^2 = 0.86$ ,  $n = 46$ ; see section S2 of the ESM). This site-specific relation was used to estimate the injection rate in the first period for INJ-1 and INJ-2, as continuous monitoring of the injection rate did not occur in this period:

$$\text{Injection rate} = 0.1449 \times \text{head rise in MW3} - 1.2301 \quad (1)$$

where the coefficients 0.1449 and 1.2301 are dimensionless. The ratio of the injection rate over the water pressure was used to monitor well performance, which is referred to as the well injectivity ( $\text{m}^3/\text{h}/\text{bar}$ ) (Brehme et al. 2018; Maliva 2020). All injection rates were normalized to 20 °C by multiplication with the term in Eq. (2) so that the effects of viscosity could be disregarded. This was done similarly by Stuyfzand and Osma (2020):

$$\text{Injection rate normalized} = \left( \frac{t + 43.1}{20 + 43.1} \right)^2 \times \text{Injection rate} \quad (2)$$

where  $t$  is the temperature of the TDW as measured with the CTD diver at MW-1 and MW-2. Furthermore, well clogging was monitored visually using the submersible camera before and after rehabilitation of each well; daily rainfall was obtained from a tipping bucket (EML, ARG100, United Kingdom); and the phreatic groundwater level was monitored in the field using a CTD diver (van Essen Instruments, the Netherlands).

### Well rehabilitation

Injection wells were rehabilitated from 2–4 February 2020 after the first injection period and on 26 November 2020 after the second injection period. Clogging material samples were taken as described in section ‘Groundwater and suspended material sampling’ during both events. Visual inspections of the well screens were performed using a submersible camera (Camtronic Inspector® 36) before and after each rehabilitation.

During both rehabilitations, the injection wells were first backflushed using a submersible pump with a flow rate of 11  $\text{m}^3/\text{h}$  for 15 min. Well screens were subsequently cleaned by high-pressure jetting (mechanical cleaning) at 100–200 bar. Simultaneously, water was discharged from the well at 3  $\text{m}^3/\text{h}$  for 55 min using a submersible pump. Finally, a post-backflush was performed (11  $\text{m}^3/\text{h}$  abstraction) for 15 min.

### Groundwater and Suspended Material Sampling

Samples were taken from the TDW, filtered material from the 40- $\mu\text{m}$  Klin disc filters, the wall lining of the standpipe, clogging material during well rehabilitation, and native groundwater. All samples were stored in the dark at 4 °C. Native groundwater was sampled from six monitoring wells with 1-m well screens from 12 to 32 m below surface level (bsl), located at 2.5 m from INJ-1. TDW was sampled from the drain reservoir, but only when drainage water was discharged in wet periods to ensure that no stagnant water was sampled. Furthermore, material was sampled from all disc filters and the inner wall of the standpipe. The condition in the collection drain was filmed using the submersible camera and afterwards it was visually interpreted. A 3-min discharge event was filmed by placing the submersible camera in the collection drain approximately 1 m from the discharge outlet. Lastly, both well rehabilitations were sampled. Jerrycans (10 L, PE) were filled with discharged water from the first backflush and the high-pressure jetting.

### Sample analysis

#### Preparation of the well rehabilitation samples

Samples from the well rehabilitation (9.3–10.7 L) were stored upright for 3–6 days, to let the suspended material settle. A large part of the fluid-fraction was removed (8.5–9.8 L; 90–99% of total volume) using a peristaltic pump and transferred to clean 10 L PE jerrycans. The wet slurry left (0.1–1.0 L) contained the solid-fraction, which was transferred to 1 L glass bottles. The fluid-fraction (section ‘Analysis of TDW, native groundwater, and the fluid-fraction



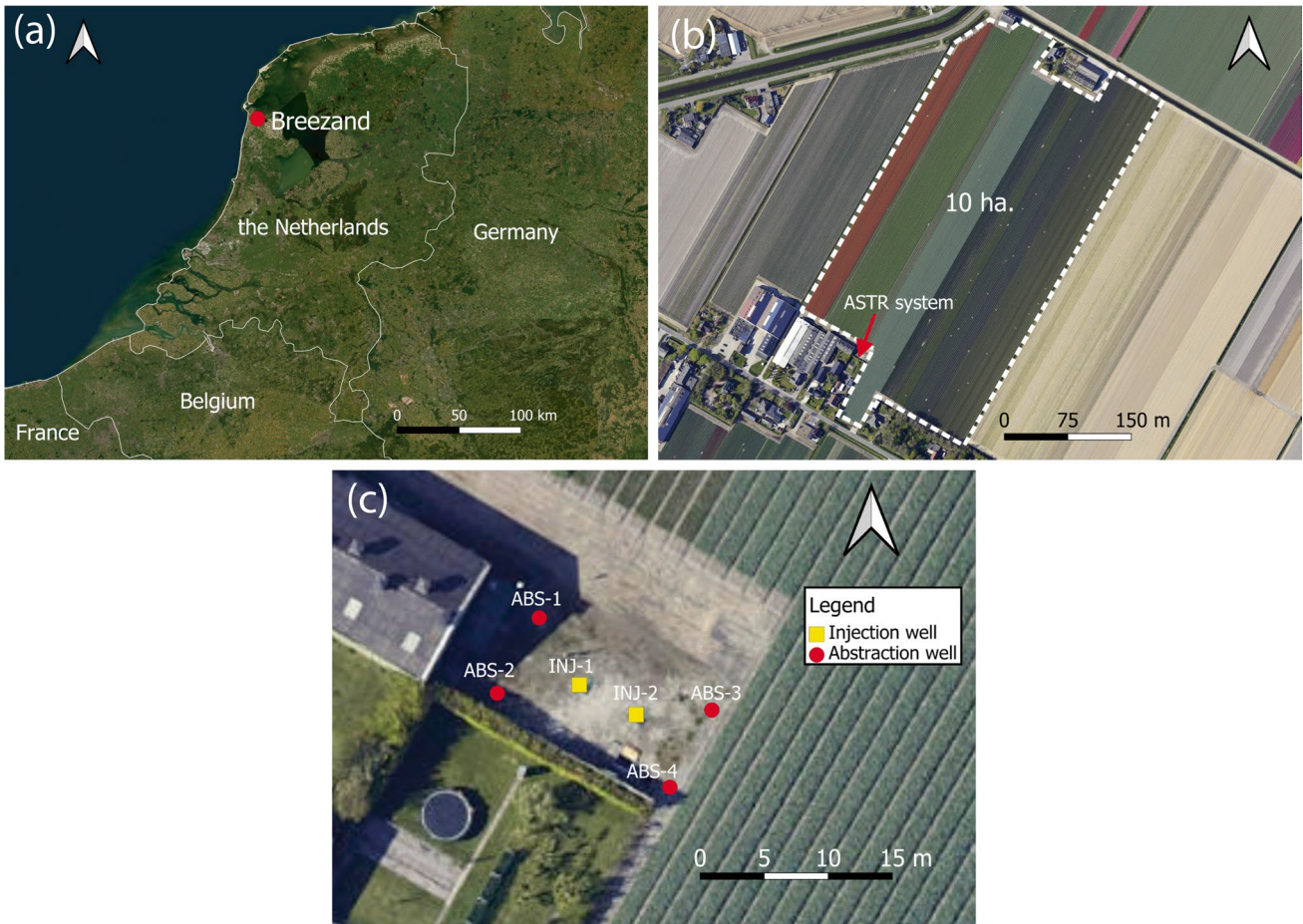


**Fig. 1** a Location of the research site (red pin) in the Netherlands. b Regional map of the field site showing the ASTR pilot and the 10-ha agricultural field in blue. c Map of the well configuration with injection wells (yellow) and abstraction wells (red)

of the well rehabilitation samples’) and solid-fraction (section ‘Analysis of the solid-fraction of the well rehabilitation samples’) were analysed separately afterwards.

**Analysis of TDW, native groundwater, and the fluid-fraction of the well rehabilitation samples**

TDW and native groundwater were sensed on EC, pH, and temperature (C4E/ PHEHT/ OPTOD, Ponsel, France) using a flow cell in the field. Well rehabilitation samples were sensed on EC, pH, and temperature (InoLab Multi 720 and InoLab Multi 9420, WTW™, Germany) in the lab, without temperature correction for EC at temperatures ranging from 11.4–12.6 °C. These EC values were converted to EC<sub>20</sub> by Eq. (3) (Stuyfzand 1993; Walter 1976):

$$EC_x = EC_t \times (1 + 0.023 \times (x - t)) \tag{3}$$

where EC<sub>x</sub> is the EC calculated at temperature x, and EC<sub>t</sub> is the EC monitored at temperature t (°C). Turbidity (NTU)

was determined by a turbidimeter (HACH 2100 N Turbidimeter, United States). For further analysis, all samples were filtered over 0.45-µm cellulose acetate membrane (Whatman Spartman 30/0.45RC syringe). Anions (Br, Cl, F, NO<sub>2</sub>, NO<sub>3</sub>, PO<sub>4</sub>, SO<sub>4</sub>) were analysed using ion chromatography (883 Basic IC Plus; Metrohm AG, Switzerland). Cations (As, B, Ba, Ca, Co, Cr, Cu, Fe, K, Li, Mg, Mn, Mo, Na, Ni, P, Pb, S, Sb, Se, Sr, Ti, V, and Zn) were analysed using inductively coupled plasma – mass spectrometry (ICP-MS; Plasma-Quant MS, Analytik Jena, Germany) after acidification with 69% HNO<sub>3</sub> (1:100). NH<sub>4</sub> (using an acidified sample) and alkalinity (using a not acidified sample) were analysed using discrete analysis (DA; Aquakem 250, Labmedics, UK). The alkalinity of the fluid-fraction of the well rehabilitation samples was not determined and was, therefore, estimated by Eq. (4) (Stuyfzand 1993):

$$X = \left| \sum a - \sum c \right| \times \frac{MW_x}{Z_x} \tag{4}$$

where  $X$  is the major constituent lacking in the ionic balance—in this case alkalinity (mg/L)— $\sum a - \sum c$  the sum of anions minus the sum of cations (meq/L), and  $MW_x$  the molecular weight of  $X$  (g/mol, and  $Z_x$  the charge of  $X$  (–). DOC was determined using a total organic carbon analyser (TOC-V CPH, Shimadzu, Japan). Mineral saturation indices were calculated for mean TDW using PHREEQC version 3.6.2 (Parkhurst and Appelo 2013). Total dissolved solids (TDS) were calculated by summing all analysed solutes, where DOC was multiplied with 2.5 to estimate dissolved organic matter.

The residue of evaporation (RE) was estimated using Eq. (5) with a factor 0.698 as done before by Stuyfzand (1993), Eq. 3.3, p. 83). Equation 6 was presented by Knudson (1901) to calculate the water density  $\rho$  (kg/L) as function of RE and temperature, suitable for EC < seawater:

$$RE = 0.698 \times EC_{20} \quad (5)$$

$$\rho = 1 + (8.05 \times 10^{-7}) \times RE - (6.5 \times 10^{-6}) \times (t - 4 + 2.2 \times 10^{-4} \times RE)^2 \quad (6)$$

#### Analysis of the solid-fraction of the well rehabilitation samples

The wet slurry left was heated in the oven at 105 °C for 72 h to evaporate the residual water. Total solids (TS) remaining originated from the fluid- and solid-fraction in the wet slurry. A digital microscope (VHX-5000 series, Keyence, Mechelen, Belgium) with 20–200× and 100–1000× magnification was used to visually inspect some of the samples. About 1 g of the total solids (TS) was crushed, homogenized, and acidified to dissolve carbonates before the analysis of organic carbon ( $C_{org}$ ; LECO Induction Furnace Instruments). From these samples, organic material (by oxidation using  $H_2O_2$  at about 100°), iron-oxides and carbonates (by acidification after the addition of HCl) were removed, and clay particles were disaggregated (by addition of tetrasodium pyrophosphate) afterwards. Lastly, these samples were analysed on sediment particle size by laser diffraction (Helos KR wet particle analyser, Sympatec GmbH, Germany). Furthermore, 30 mg of homogenized crushed material was analysed for elemental composition after digestion (APHA method 3030E). The digested substance was diluted to 100 ml with ultra-pure water. From this sample, a subsample was taken which was diluted (1:50), acidified with 69%  $HNO_3$  (1:100), filtered over 0.45  $\mu m$ , and analysed for major cations (Ca, Fe, Mn, P, Al) by ICP-MS.

Each chemical constituent was corrected for mineral and salt formation during evaporation of the remaining fluid fraction as similarly done by Stuyfzand and Osma (2019). First, the weight ratio of chemical constituent  $X$  (%) was

estimated by Eq. (7), using the concentration of constituent  $X$  (mg/L) and total digested material (mg):

$$\text{Weight ratio } X = \frac{\text{constituent } X \times 0.1}{\text{digested material}} \times 100 \quad (7)$$

Second, the weight of the chemical constituent  $X$  (mg) as part of the TS was calculated by Eq. (8):

$$X_{TS} = \frac{\% \text{ weight ratio } X}{100} \times \text{TS per sample} \quad (8)$$

Third, the weight of the chemical constituent  $X$  (mg) in water was estimated by multiplying the concentration of constituent  $X$  in the fluid fraction (mg/L) with the evaporated volume (L) using Eq. (9):

$$X_{H_2O} = \text{constituent } X \text{ in fluid fraction} \times \text{evaporated volume in slurry} \quad (9)$$

Finally, the fraction (% dry wt) of chemical constituent  $X$  in the total suspended solids (TSS; mg) was calculated after correction for the remaining fluid fraction by Eq. (10):

$$X_{TSS} = \frac{X_{TS} - X_{H_2O}}{TSS} \times 100 \quad (10)$$

#### Analysis of bacterial communities by 16S rRNA analysis

Suspended solids were filtered from the well rehabilitation water samples using Nalgene reusable filter units (Thermo Scientific). Powerbead tubes (Qiagen) disintegrated the fraction of biomass in the suspended solids, after which the environmental DNA was extracted following the manufacturer's instructions using the DNeasy PowerLyzer PowerSoil Kit (Qiagen). The Qubit 4 Fluorometer (ThermoFisher) quantified the extracted DNA. Extracted DNA was afterwards sent for 16S ribosomal RNA (rRNA) sequencing to Novogene (Hongkong). The universal primers 341F (5'- CCT ACG CGA GGC AGC AG) and 517r (5'- ATT ACC GCG GCT GCT GG -3') targeted the V3–V4 hypervariable region (Muyzer et al. 1993), which was sequenced with the Illumina HiSeq paired-end platform generating paired-end raw reads of 400–450 bp. The quality of the sequences (base calling, base composition, guanine-cytosine (GC) content) was checked using FastQC (Andrews 2010). The pipeline QIIME (version: 1.9.1; Caporaso et al. 2010) performed the selection of 16S rRNA genes, clustering, and OTU picking and taxonomic classification. The chimeric sequences were removed using de novo chimera method in UCHIME implemented in the tool VSEARCH. The processed reads from both libraries were pooled and clustered into operational taxonomic units (OTUs), using the Uclust program (similarity cutoff = 0.97). Representative sequences were identified

for each OTU and aligned against the SILVA database using the PyNAST program (Caporaso et al. 2010). An unrooted Neighbor-Joining (NJ) tree was constructed of the 32 predominant bacterial 16S rRNA gene sequences using the software MEGA X version 11 (Tamura et al. 2021). The raw sequencing data have been submitted to the NCBI Sequence Read Archive; accession number PRJNA809926 (Delft University of Technology 2022).

## Results and Discussion

### Tile drainage water and native groundwater characteristics

The native groundwater was brackish and deeply anoxic in the target aquifer. Salinity gradually increased with depth ( $EC = 1,860\text{--}9,830 \mu\text{S/cm}$ ).  $O_2$  and  $NO_3$  were absent.  $Fe^{2+}$  concentrations ranged between 9.5–39 mg/L;  $SO_4:Cl$  ratios ( $\frac{\text{mg/L}}{\text{mg/L}}$ ) were 0.002–0.0005 and substantially lower than sea water ( $\sim 0.14$ ), being the source of the native brackish groundwater; while methane concentration ranged between 11 and 40 mg/L. These groundwater compositions point to both Fe- and  $SO_4$ -reducing and methanogenic redox conditions.

Tile drainage water (TDW) was fresh ( $EC = 1,293 \pm 397 \mu\text{S/cm}$ ), nutrient-rich, and (sub)oxic ( $O_2 = 6.4 \pm 1.9 \text{ mg/L}$ ). High nutrient concentrations ( $NO_3$ :  $14.1 \pm 11.3 \text{ mg/L}$ ;  $PO_4$ :  $5.21 \pm 0.80 \text{ mg/L}$ ;  $NH_4$ :  $0.13 \pm 0.11 \text{ mg/L}$ ) originate from agricultural fertilizers. Degradation of organic matter likely results in reduction of  $O_2$  in the top soil, while TDW is mostly oxygenated in the not fully saturated tile drains and drain reservoir. The presence of particulate Fe-(hydr)oxides in TDW was indicated by the higher Fe concentration in the unfiltered ( $Fe = 0.43 \text{ mg/L}$ ) vs. filtered ( $Fe = 0.17 \text{ mg/L}$ ) TDW sample collected before injection in May 2020. High-frequency (every 10 min) turbidity measurements levelled between 5 and 20 NTU after filtration by the disc filters, with extremes up to 165 NTU. The mean temperature of TDW was  $10.1 \text{ }^\circ\text{C}$ , with a maximum of  $14.5 \text{ }^\circ\text{C}$  observed in autumn and a minimum of  $9.0 \text{ }^\circ\text{C}$  in winter. Mean values of mineral saturation indices (SIs) in TDW (see section S3 of the ESM) were supersaturated for various minerals consisting of Ca and/or Fe and/or  $PO_4$ : calcite ( $CaCO_3$ ,  $SI = 0.3$ ), ferrihydrite ( $Fe(OH)_3$ ,  $SI = 1.3$ ), Fe-hydroxyphosphate ( $Fe_{2.5}PO_4(OH)_{4.5}$ ,  $SI = 15$ ), and hydroxyapatite ( $Ca_5(PO_4)_4(OH)$ ,  $SI = 3.0$ ). Note that the tile drainage network is constructed in a shell bed, which likely led to (super)saturated conditions for calcite and hydroxyapatite as a result of the enriched Ca concentrations plus the high  $PO_4$  concentrations in TDW. Further

information on the composition of TDW is presented in section S3 of the ESM.

Figure 2 displays microscope images of materials obtained from the 40- $\mu\text{m}$  disc filters and from the standpipe after injection period 2 in November 2020. These materials likely consist of Fe-oxidizing bacteria (FeOB), as, first, filamentous morphologies and structures are observed similar to FeOB (Emerson and De Vet 2015; Krepski et al. 2012). Second, iron-oxides were present as shown by a simple acidification test ( $pH < 3$ ; 1%  $HNO_3$ ) on the suspended material, which resulted in a substantial decline in the volume of the bulk material (section S4 of the ESM). Third, a metallic sheen was observed in the standpipe on top of the stagnant water surface—after 41 days of standstill, after injection period 2 in November 2020 (section S5 of the ESM), which indicates the presence of FeOB (Emerson and De Vet 2015). The interior of the standpipe was covered by a thick structure of most likely Fe-precipitates and microbial deposits, which was observed after submerging the camera in the standpipe (section S6 of the ESM). A similar structure was observed on the lining of the inner wall of the outlet of the collection drain to the drain reservoir (section S7 of the ESM). The relation with FeOB seems likely, as Süsser and Schwertmann (1983) also observed bacterial oxidation of Fe(II) in drainpipes. The observed particles in the microscope images can be mineral precipitates like Fe-(hydr)oxides, hydroxyapatites, or calcite (as being (super)saturated in TDW), but also silts and/or clay particles.

Table 1 presents clogging mitigation guidelines from the literature and compares them with the mean water quality composition of TDW. Biological clogging was thus likely to occur in the current research, as the guidelines of DOC, nutrients, and oxidants ( $O_2$  and  $NO_3$ ) were largely exceeded. Furthermore, physical clogging was also expected as (1) turbidity levels were above the recommended value, and (2) suspended material  $< 40 \mu\text{m}$  can pass the disc filters.

### Extent of the Clogging Problem

Figure 4 presents daily rainfall, phreatic groundwater levels in the agricultural field, hydraulic heads in the aquifer at MW-1 and MW-3, turbidity in the standpipe after TDW passed the 40- $\mu\text{m}$  disc filters, and the normalized well injectivity calculated for INJ-1. These data were used to analyse and describe the extent of clogging in INJ-1. The data for INJ-2 is presented in section S8 of the ESM and is only briefly discussed in this section, as clogging in INJ-1 and INJ-2 developed in a similar way. However, the hydraulic



head rise in MW-1 was generally lower than in MW-2 (corresponding to INJ-1 and INJ-2, respectively) during the second and third injection period, while the flow was about the same. This could be caused by small variations in hydrogeology and/or the quality of the well construction.

### Injection period one

At the start of operation, the highest normalized well injectivity ( $\sim 5.5 \text{ m}^3/\text{h}/\text{bar}$ ) was observed. The injectivity gradually decreased afterwards, due to clogging. Frequent short injectivity peaks showed that only small volumes were injected from 28 November 2019 until 6 December 2019. In this period, the normalized well injectivity decreased, indicating well clogging. From 6 December 2019 until the end of period one on 11 December 2019, heavy rainfall events provided larger volumes for injection. The large TDW discharge coincided with increasing turbidity (measured after the disc filters) and resulted in a substantial head increase in MW-1. The inside of the collector drain was filmed and it was observed that it was covered with a mat of probably Fe-precipitates and microbial deposits (section S7 of the ESM). The turbidity increase likely resulted from the high water pressures and flow velocities in the drain related to the large rainfall event. This induced the mobilization of precipitates and microbial deposits. Concurrently, the hydraulic head in MW-3 at 7 m distance from INJ-1 decreased. The head increase in MW-1 suggested clogging of the well screen or the borehole wall, which matched with the lower head in MW-3 caused by a lower injection rate. The normalized well injectivity largely reduced ( $5.5$  to  $2 \text{ m}^3/\text{h}/\text{bar}$ ) during the 23 days of operation in injection period 1, which indicated that the wells got quickly clogged. Figure 3a depicts the clogged state after injection period 1 from screenshots of video footage of the interior of INJ-1. The full screen (21.5 m) showed internal well staining of predominantly orange/brown and black/Gy materials. Based on the video footage, it was roughly estimated that approximately 95% of the screen slots were filled. It seems very likely that the borehole wall is also clogged to some extent, besides the clogging of the well screen.

### Injection period two

After injection period one, well screens were rehabilitated and an automated backflush system was installed in both injection wells with the aim to limit clogging. Note, that the injectivity did not return to its initial value of injection period 1. This suggests that the borehole wall and aquifer were still partially clogged, in contrast to the well screen as video footage shows clean filter slots (Fig. 3b). During injection period 2, automated backflush events resulted in a more stable injectivity between 20 September 2020 and 3 October

2020 (Fig. 4); however, from 6 October 2020 until the end of injection period 2, injectivity substantially decreased from  $3.5$  to less than  $2 \text{ m}^3/\text{h}/\text{bar}$ , during a severe rainfall event ( $\sim 45 \text{ mm}$  in 3 days). The hydraulic head increased in INJ-1, which later abruptly decreased. The increase in hydraulic head must have been related to clogging of the well screen and/or the borehole wall, which is probably caused by the high turbidity of the TDW injected during and after the rainfall event. The abrupt decrease in hydraulic head probably resulted from clogging of the disc filters, due to a large influx of suspended materials. Visual inspections showed that the disc filters were fully clogged, and the filter backflush system was not able to clean the filters anymore.

### Injection period three

Well screens were again rehabilitated before the start of injection period 3, using the same rehabilitation methods as after injection period 1. As an additional precautionary measure, this time a turbidity sensor was installed in the drain reservoir, which together with the controller regulated that only TDW with a turbidity below a set maximum value ( $< 20 \text{ NTU}$ ) was used by the ASTR system. TDW with a turbidity  $> 20 \text{ NTU}$  was thus discharged to the surface-water system. Injectivities during injection period 3 were comparable to the initial injectivities of injection period 2, which suggests that the borehole wall and aquifer did not get further clogged during injection period 2. Observed hydraulic heads and injectivities were relatively stable during period 3. The large rainfall event at 9 March 2021 ( $\sim 35 \text{ mm}$  in 1 day) did not immediately decrease injectivity as observed in injection period 2. Zuurbier and van Dooren (2019) observed increased well injectivity after a 30-day standstill at another ASR site in the Netherlands, which they assigned to microbial die-off. However, a 33-day standstill in January 2021 (injection period 3) did not increase normalized well injectivity in the current study, which suggests that biological clogging is not the main clogging mechanism.

## Diagnosing the main clogging mechanisms

### Clogging material composition

Clogging material of INJ-1 and INJ-2 was sampled during the first rehabilitation event (backflush and high-pressure jetting); unfortunately, however, the backflush samples comprised insufficient total suspended solids (TSS) for elemental analysis. Table 2 shows an overview of the composition of the suspended matter in the samples obtained during high-pressure jetting. The analysis could retrieve only between 3.3–16.8% of the weight of the TSS; thus, a large part is not identified, because (1) not all materials were digested



(mainly quartz) before analysis, (2) some major elements were not analysed (especially S and Si, due to restrictions of the laboratory analysis), and (3) the element contents were not converted to their oxide, hydroxide, or mineral form in which they are naturally observed in aquifers. The main constituents in the suspended matter are, in decreasing order, Fe,  $C_{org}$ , P, Ca, Al, Mn. From these constituents, contents of  $C_{org}$ , Fe, P, and Mn were mostly substantially larger than observed in the aquifer sediments (Table 2), indicating that they originate from the clogging material in the well and thus not from the aquifer.  $C_{org}$  likely originates from organic matter residues from the crops or top soil, or from biomass grown in the well and is related to biological clogging. Fe contents are probably related to Fe-(hydr)oxides, Fe-sulphide, and Fe- $PO_4$  precipitates (Stuyfzand and Osma 2019). The latter also partly explains the observed P contents; however, P could partially also originate from organic matter. Observed Mn contents are likely from Mn-(hydr)oxides. In INJ-1, samples were taken during the downward movement of the jetting nozzle. The sequence of samples (HD1–HD5) therefore represents increasingly larger depths; however, the specific depth of the abstracted water cannot be determined. Contents of specific constituents did not correlate with depth.

The particle size distribution was determined for a sample taken during backflush and a sample taken during high-pressure jetting (HD3, INJ-1; Fig. 5). The distribution showed two distinct peaks for the backflush sample—at 10 and 200  $\mu\text{m}$ . The 10- $\mu\text{m}$  peak was not observed in the distribution of the sample collected during high-pressure jetting, indicating that the materials from the 10- $\mu\text{m}$  peak do not

originate from the aquifer, as this peak would otherwise be expected at both samples. The 10- $\mu\text{m}$  peak likely represents clays and silts that have passed the disc filters (<40  $\mu\text{m}$ ) and resulted in physical clogging of the well screen. Note that materials >40  $\mu\text{m}$  cannot pass the disc filter and must therefore come from the aquifer.

### Hydrochemical environment in the well

Water compositions remarkably varied between the backflush samples of INJ-1 over time, as described in the following. The composition of the first backflush samples represented the standing well volume and the later samples the water in the aquifer. Note, that the ASTR system was idle for  $\pm 2$  months before these samples were taken between injection periods 2 and 3. The standing water in the well was deeply anoxic, as  $O_2$  and  $NO_3$  were absent. Moreover, a ‘rotten egg’ smell was noticed when removing the well heads before sampling; the smell of  $H_2S$  indicates a  $SO_4$ -reducing environment. This coincides with the 20% lower  $SO_4$  concentrations measured in the standing water of the well compared to the aquifer water sampled at INJ-1 ( $SO_4$ : 160 vs. 200 mg/L). Furthermore,  $Fe^{2+}$  (3,500 vs. 45  $\mu\text{g/L}$ ) and  $Mn^{2+}$  (580 vs. 420  $\mu\text{g/L}$ ) concentrations were elevated in the standing water in the well, which suggests reductive dissolution of Fe- and Mn-(hydr)oxides in the well during standstill. Stuyfzand et al. (2006) and Vanderzalm et al. (2006) also observed increases of DOC,  $Fe^{2+}$ ,  $Mn^{2+}$ ,  $NH_4$ , and P concentrations in the standing water in the well they investigated, which were likely caused by the decay of biomass in the well. Mayer and Jarrell (2000) concluded that

**Fig. 2** Microscope images of suspended material retained from **a** the 40- $\mu\text{m}$  disc filters and **b** the standpipe. The images show brownish filamentous structures and black particles

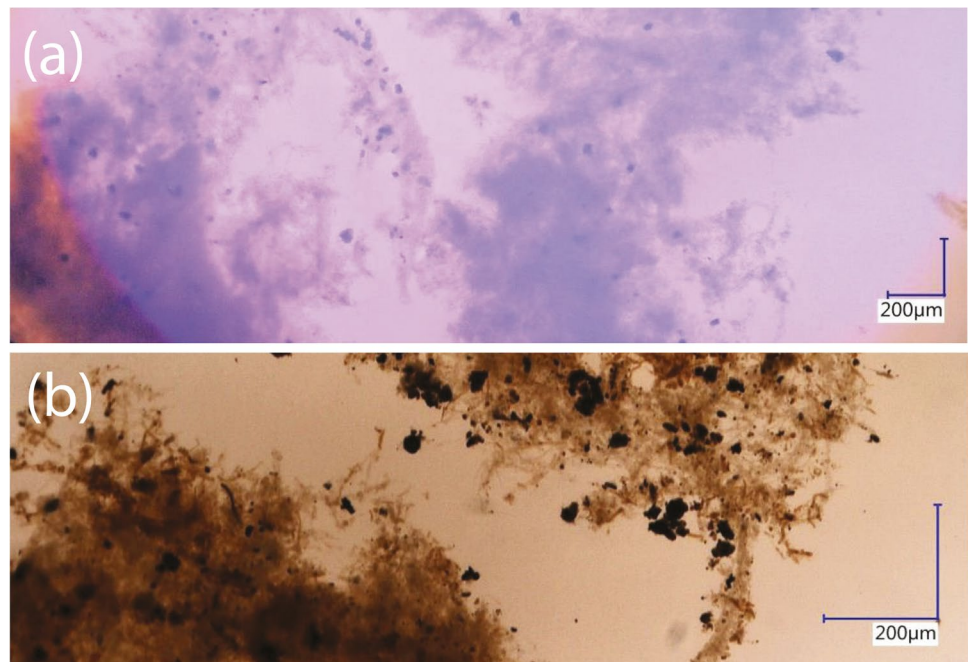


**Table 1** Overview of clogging mitigation guidelines in comparison to the mean water quality composition of TDW

| Clogging mitigation parameter      | Literature parameters |   | Mean TDW concentration |
|------------------------------------|-----------------------|---|------------------------|
|                                    | Recommended value     | Source  |                        |
| Turbidity (NTU)                    | <5                    | Martin (2013)                                     | 5–165                  |
| Total iron ( $\mu\text{g/L}$ )     | <10                   | Zuurbier and van Dooren (2019)                    | 430                    |
| DOC ( $\text{mg/L}$ )              | <2                    | Zuurbier and van Dooren (2019)                    | 24.7                   |
| Ammonium ( $\text{mg/L}$ )         | <0.5                  | Hubbs (2006)                                      | 0.13                   |
| Phosphate ( $\text{mg/L}$ )        | Low                   | Stuyfzand and Osma (2019)                         | 5.2                    |
| Nitrate ( $\text{mg/L}$ )          | Low                   | Eom et al. (2020)                                 | 14.1                   |
| Dissolved oxygen ( $\text{mg/L}$ ) | Low                   | Stuyfzand, TU Delft, personal communication, 2021 | 2–6                    |
| Sodium Adsorption Ratio (–)        | <6                    | Zuurbier and van Dooren (2019)                    | 1.40                   |

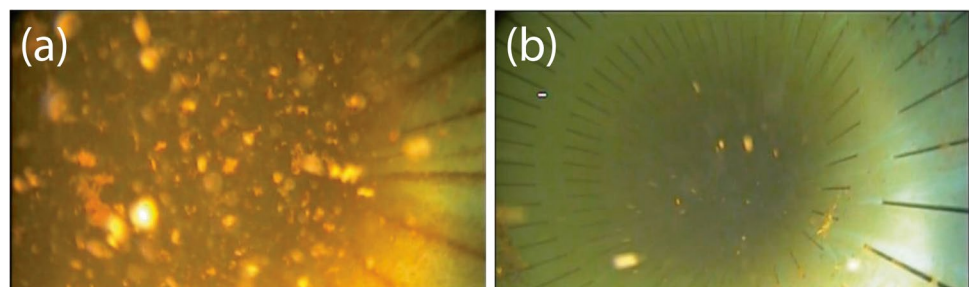
P mobilization can also be associated with a reductive dissolution of iron-oxides in which P is co-precipitated.  $\text{PO}_4$  and DOC also showed elevated concentrations in the standing water in the well in the current study (respectively;  $\text{PO}_4^{3-}$ : 37 vs. 12  $\text{mg/L}$  and DOC: 48 vs. 25  $\text{mg/L}$ ). Therefore, it was also expected that the strongly anoxic conditions are related to decay of biomass within the well.

### Bacterial communities

Bacterial communities were analysed using metagenomics in two samples taken from the standpipe (sample SP) and the clogged well (sample CW) during the second rehabilitation. Chemical analysis showed variations in the oxidative conditions between these samples, which resulted in selective sustenance of the bacterial population. The metagenomic library datasets from the partially oxic standpipe sample (SP) and anoxic clogged well sample (CW) were clustered and results are presented in Fig. 6.

TDW resides in the standpipe after filtration by the disc filters, and was aerobic, as the standpipe contains openings to the atmosphere. The standpipe was always partly filled with TDW and was only flushed during ASTR injection. A sample was taken of the wall lining of the standpipe (Fig. 2, and sections S5 and S6 of the ESM). This sample was dominated by methylothrophic (methane degraders/consumers) microbes such as *Nitrospira*, *Methylotenera*,

*Crenothrix*, *Methylomona*, *Methanosaeta*, and *Methylobacter*, indicating the use of  $\text{CH}_4$  as their electron donor, which can also trigger the reductive dissolution of Fe(III) minerals (Glodowska et al. 2020; Jorgensen 1989). However, the predominant genera *Crenothrix* is known as a  $\text{CH}_4$ -oxidizing and Fe-oxidizing bacteria (Stoecker et al. 2006) and *Nitrospira* as a  $\text{NO}_2$ -oxidizing bacteria (Bayer et al. 2021), symbiotically supporting  $\text{NO}_3$  dependent Fe-oxidation processes (Fig. 6). Furthermore, the standpipe sample presented  $\text{NH}_4$ -oxidizing groups like *Nitrosoarchaeum* and the co-dominance of  $\text{NO}_2$ -oxidizers like *Nitrospirae*, which can compete with  $\text{CH}_4$ -oxidizers (such as *Methylotenera*, *Methylomonas*) for nitrogen sources (Daebeler et al. 2014). The denitrifying bacteria *Polynucleobacter* provides a symbiotic balance to both the groups.  $\text{NO}_3$  in TDW was the main N source in the system, and this caused the existence of denitrifying bacteria, nitrite oxidizers, and ammonium oxidizers. Overall, a high rate of biological activity was induced by the DOC and  $\text{NO}_3$  available in TDW, resulting in an abundance of bacterial groups involved in C and N metabolism and iron oxidation in the standpipe. The conditions in the wall lining of the standpipe seemed (highly) anaerobic based on the observed genera, despite the aerobic TDW residing in the standpipe. In this sample, a very high predominance of *Cenothrix* confirmed the filamentous and sheathed structures observed microscopically (Fig. 2).

**Fig. 3** Screenshots from video footage of the interior of INJ-1 after injection period 1, which depict the well screen **a** before rehabilitation, and **b** after rehabilitation, both taken on 2 February 2020 at 15-m depth

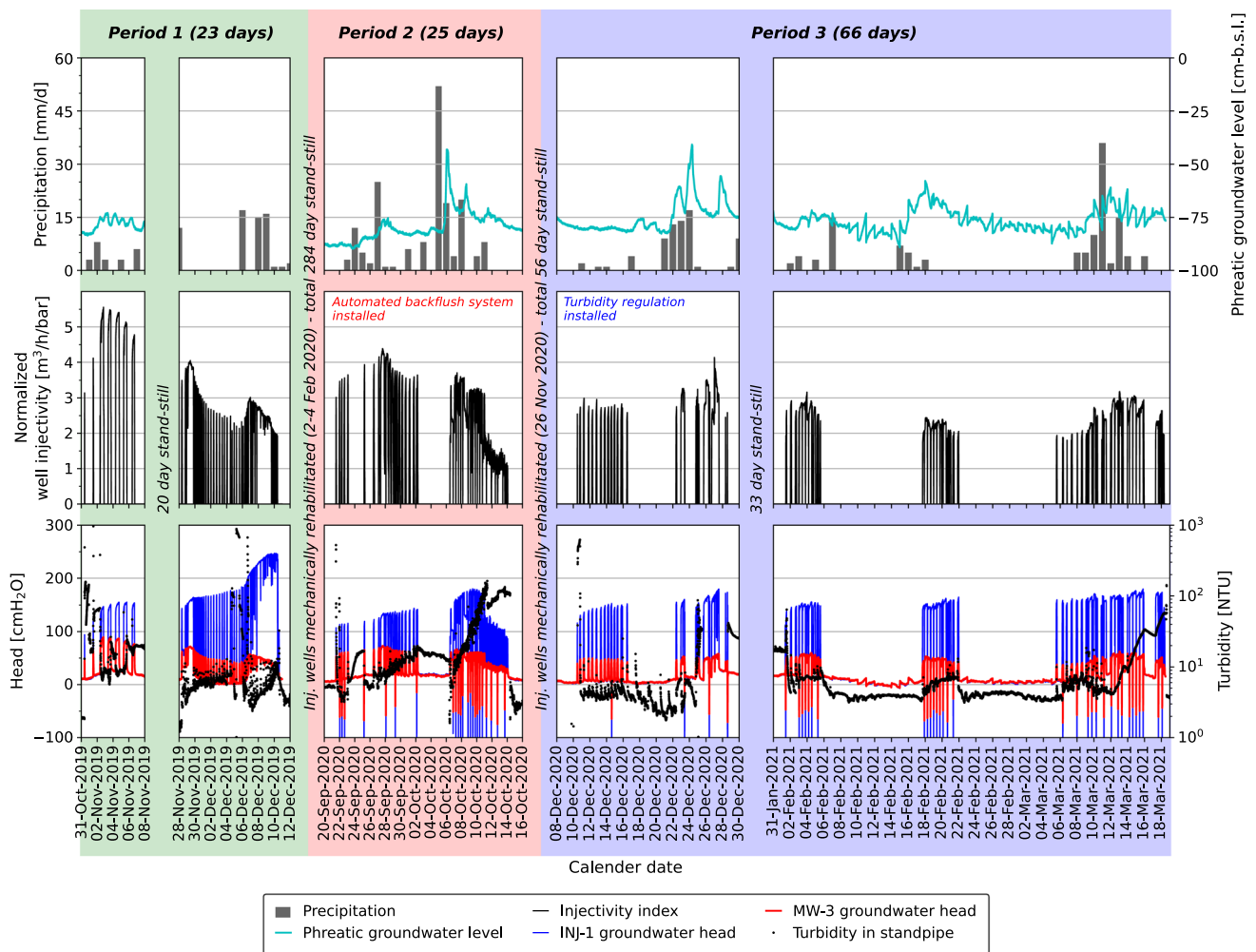


**Fig. 4** Data obtained during injection period 1 (green panel; 23 days of injection), period 2 (red panel; 25 days of injection), and period 3 (blue panel; 66 days of injection). They show rainfall (mm/day), phreatic water level in the field (cm bsl), normalized injectivity index ( $\text{m}^3/\text{h}/\text{bar}$ ) of INJ-1, observed groundwater head ( $\text{cmH}_2\text{O}$ ) in INJ-1

(measured in MW-1) and MW-3 at 7 m from INJ-1, and turbidity level (NTU) of injected water after the disc filters measured in the standpipe. No data on phreatic water level could be gathered between 29 November and 11 December 2019 (first injection period)

The CW (clogged well) sample showed a high abundance of methanogenic microbes (*Methanosaeta*, *Methanoregula*, *Methylomonas*, *Methalomonas*) along with Fe(III) reducers (*Rhodoferrax*, *Ferribacterium*, *Pseudomonas*, *Acidovorax*). Also, an abundance of nitrate reducing - Fe(II) oxidisers (*Gallionella* and *Acidovorax*) was observed. During Fe-oxidation, the end product Fe(III) can inhibit methylogenes (Reiche et al. 2008); however the presence of methanogenic bacterial groups suggested otherwise. Their presence probably related to the coagulation and clogging by the exopolysaccharide producing filamentous microbes like *Arcobacter*, *Trichococcus*, *Pseudoarthobacter*, *Burkholderia*, and *Gallionella*, which trapped the Fe(III) by producing bacterioferritin-Fe(III)-exopolysaccharide complexes in the system (Rivera 2017). The presence of *Sulfurimonas* and *Sulfuricum* indicated  $\text{NO}_3$  reduction coupled to sulphur and

hydrogen oxidation, which was reflected by the absence of  $\text{NO}_3$ . However, the presence of sulfur reducing genera such as *Sulfospirillum* and *Desulfovibrio* caused the reduction of this  $\text{SO}_4$ , probably causing the smell of ‘rotten eggs’ during sampling. Interestingly in this sample, clogging did not only result from the filamentous mesh formed by Fe(II) oxidizers, but also from stabilizing iron-sequestering protein (bacterioferritin, siderophore), which were formed by filamentous bacterial groups such as *Burkholderia*, *Gallionella*, and *Nocardiodes* (Schneider et al. 2007; Tuomanen et al. 2000). Furthermore, Fe(III) is trapped by the biopolymer produced by the groups (*Arcobacter*, *Trichococcus*, *Pseudoarthobacter*, *Burkholderia*, *Gallionella*), which makes the biomass a robust and dense iron oxide matrix (Fig. 3).

The bacterial communities of both samples showed an abundance of genera which are involved in the metabolism

of C and N and Fe-oxidation. The functional analysis of the communities corresponds with the visual images obtained with a microscope (Fig. 2 and section S6 of the ESM) and the camera footage within the well (Fig. 3). One can therefore conclude that biological clogging plays a role during well clogging. The influence of biological clogging could be decreased by lowering the concentrations of nutrients (C, N, P) and Fe in the TDW, which is, however, very difficult to realize in a low-cost way.

### Impact of precautionary clogging-prevention measures on ASTR performance

Figure 7 shows the normalized well injectivity versus the cumulative turbidity load after the disc filters—turbidity (NTU) × injected volume (m<sup>3</sup>). The turbidity load relates to the total number of particles injected; therefore, the figure shows the relation between well clogging and the number of particles injected. Each data point represents a monitoring time step of 30 min. It is possible that injection was switched on and off within this monitoring time step. The calculated normalized injectivity would then be too low, as it would be calculated as the mean of the preceding period when injection occurred and the subsequent period that the pump was turned off (or the other way around). To take out these erroneous values, all data points were deleted where the injectivity was 0 in the 30 min before and after the monitoring

time step studied. Note that the figure still contains some data points that are lower than the main trend. These outliers are likely caused by the ASTR system, which turned both on and off within one monitoring time step of 30 min. The mean normalized well injectivity is, therefore, lower during these time steps. For further interpretation, the focus is on the main trend of the high-level normalized well injectivities observed.

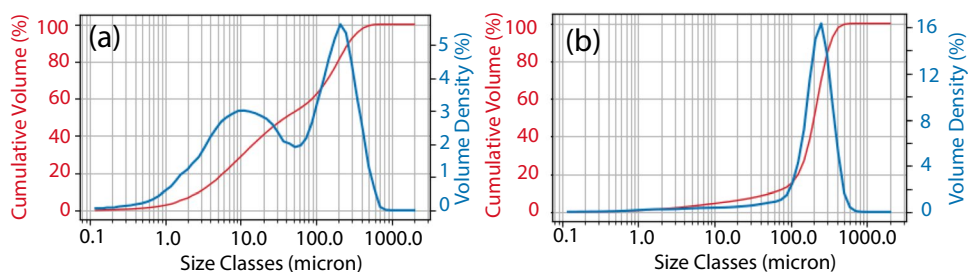
In injection period 1, normalized injectivities decreased quickly compared to the other injection periods. This showed that the TDW composition is not suitable for injection with only the 40-µm disc filter treatment. In injection period 2, wells were periodically backflushed. This was an effective measure, as the injectivity declined significantly slower compared to injection period 1, while a similar number of particles were injected. Injectivities suddenly dropped after a cumulative turbidity load of 30,000, which was not related to the pump capacity, but rather coincides with clogging of the disc filters. Injection period 3 shows a similar trend as injection period 2. At the end of the period injectivities drop, however, this does not relate to clogging but to a decrease in pump capacity related to a large precipitation event. A considerable difference is that in injection period 3, a larger amount of water was injected (2,150 m<sup>3</sup>) compared to injection period 2 (1,450 m<sup>3</sup>) for the same cumulative turbidity load, as only water was injected with a NTU <20. Therefore, turbidity regulation of TDW shows to be a powerful method

**Table 2** Overview of the constituent contents in suspended solids obtained during high-pressure jetting in injection wells 1 and 2, which are compared to the mean constituent contents in the aquifer

| Constituent      |          | Injection well 1 (INJ-1) |             |             |             |             | Injection well 2 (INJ-2) | Aquifer |       |
|------------------|----------|--------------------------|-------------|-------------|-------------|-------------|--------------------------|---------|-------|
|                  |          | HD1                      | HD2         | HD3         | HD4         | HD5         | HD1                      | Min     | Max   |
| TSS              | mg/L     | 294                      | 445         | 6558        | 376         | 2243        | 242                      | –       | –     |
| C <sub>org</sub> | % dry wt | <i>1.99</i>              | <i>2.26</i> | <i>1.14</i> | <i>5.16</i> | <i>1.68</i> | <i>4.03</i>              | 0.02    | 1.47  |
| Fe               | % dry wt | <i>2.73</i>              | <i>2.63</i> | <i>0.35</i> | <i>6.22</i> | <i>1.96</i> | <i>6.24</i>              | 0.31    | 1.29  |
| P                | % dry wt | <i>1.47</i>              | <i>1.46</i> | <i>0.21</i> | <i>3.57</i> | <i>0.61</i> | <i>3.40</i>              | 0.03    | 0.13  |
| Ca               | % dry wt | <i>0.0</i>               | <i>0.74</i> | <i>1.52</i> | <i>1.46</i> | <i>3.72</i> | <i>0.12</i>              | 0.09    | 3.97  |
| Al               | % dry wt | <i>0.13</i>              | <i>0.15</i> | <i>0.12</i> | <i>0.24</i> | <i>0.41</i> | <i>0.28</i>              | 1.79    | 6.54  |
| Mn               | % dry wt | <i>0.03</i>              | <i>0.05</i> | <i>0.01</i> | <i>0.14</i> | <i>0.05</i> | <i>0.27</i>              | <0.01   | 0.04  |
| Sum              | %        | 6.2                      | 7.3         | 3.3         | 16.8        | 8.4         | 14.3                     | 2.23    | 13.57 |

Constituents in clogging material with contents higher than maximally observed in the aquifer are shown in *italic*

**Fig. 5** Particle-size distribution of the total suspended solids (TSS) obtained **a** during back-flush, and **b** from high-pressure jetting. The red line displays the percentage cumulative volume of the sediments and the blue line the percentage volume density





to prevent injection well clogging, especially in combination with periodic backflushing of the injection wells.

**Potential alternatives to prevent clogging of this ASTR system**

Water quality could be increased using other measures to intensify or replace the current clogging-prevention measures—for example, disc filters could be installed with smaller pore sizes. Stuyfzand and Osma (2019) treated recycled injection water with 20-µm spin Klin disc filters, followed by a 1-µm bag filter. Disadvantages are the higher costs of the system and its maintenance. Note that the 1-µm bag filter clogged within 2 days during the study by Stuyfzand and Osma (2019), while the injected recycled injection water was of a better quality (e.g., turbidity <3 NTU) than the injected TDW in the current study. The most studied and applied treatment step in AS(T)R is a slow sand filter preceded by a rapid sand filter, which was successfully used at the former 2.3-ha ASTR pilot site. Zuurbier et al. (2014) and Camprovin et al. (2017) also successfully treated source waters with slow sand filters before injection. Slow sand filters have the advantage that biological processes (such as

aerobic respiration, and iron and organic matter oxidation) occur which are beneficial to prevent well clogging, besides the physical removal of particles (Maliva 2020). The disadvantage of slow sand filters is the large space needed above ground besides additional costs.

Generally, injection wells will get clogged slowly over time, despite all measures to prevent clogging; therefore, well rehabilitation remains essential. In the current study, two well rehabilitations were performed based on backflushing and high pressure well jetting of the well screen. Video footage of the wells showed that the slots of the well screen were opened after rehabilitation, but the injectivity did not return to its initial value; thus, it was suspected that the wellbore skin (borehole wall and nearby aquifer) was not fully rehabilitated. For future rehabilitations, ‘compressed air juttering’ is recommended. The groundwater level in the well is strongly lowered using compressed air during this method, and rises quickly when the pressure is released (Olsthoorn 1982). This routine is repeated until most particles from the well screen, borehole wall, and area near the well are removed. Note that air bubbles may get stuck in the vicinity of the well and could therefore also limit injectivity.

**Fig. 6** A taxonomic heat map showing the distribution of the common and predominant (in both libraries) top 32 bacterial genera in the two samples. The phylum corresponding to each genus is represented in the left column. The two right columns show the abundance of these bacteria in the samples shown by a color gradient, which indicates the distance between the raw score of the sequences and the standard deviation (blue is abundant and red is not abundant). CW is the clogged well sample and SP is the standpipe sample

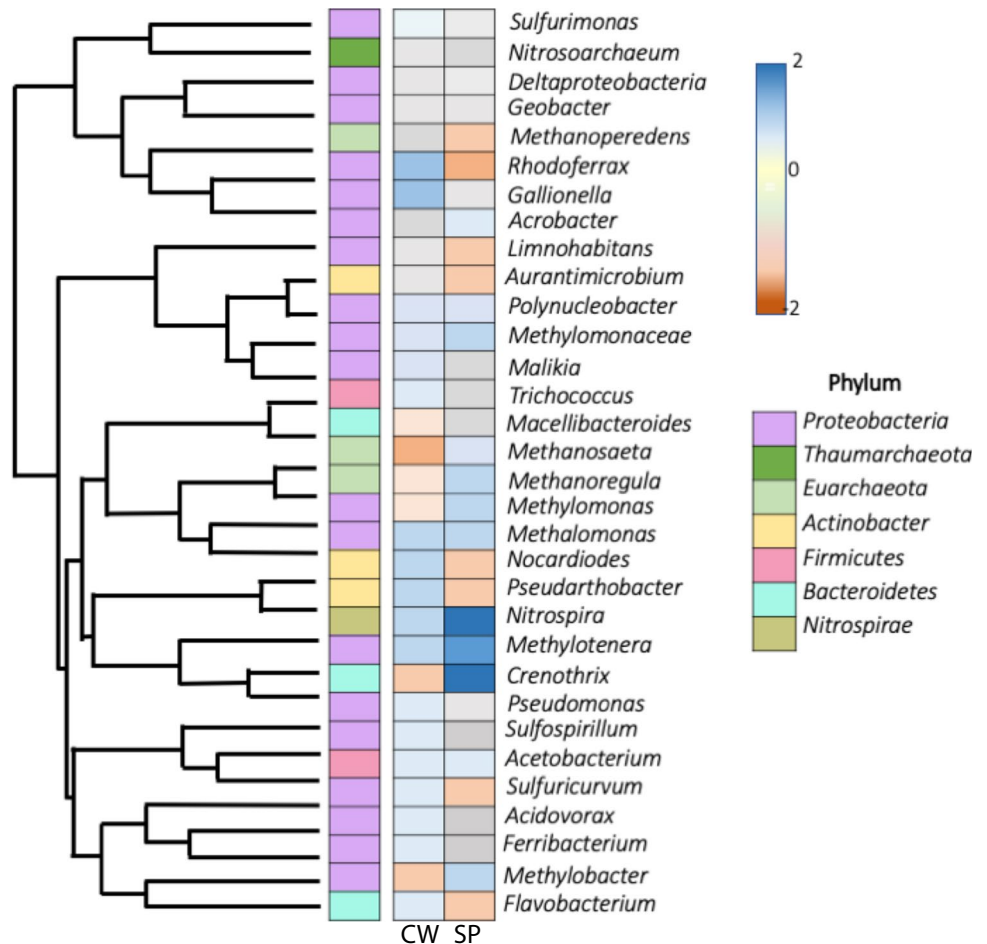
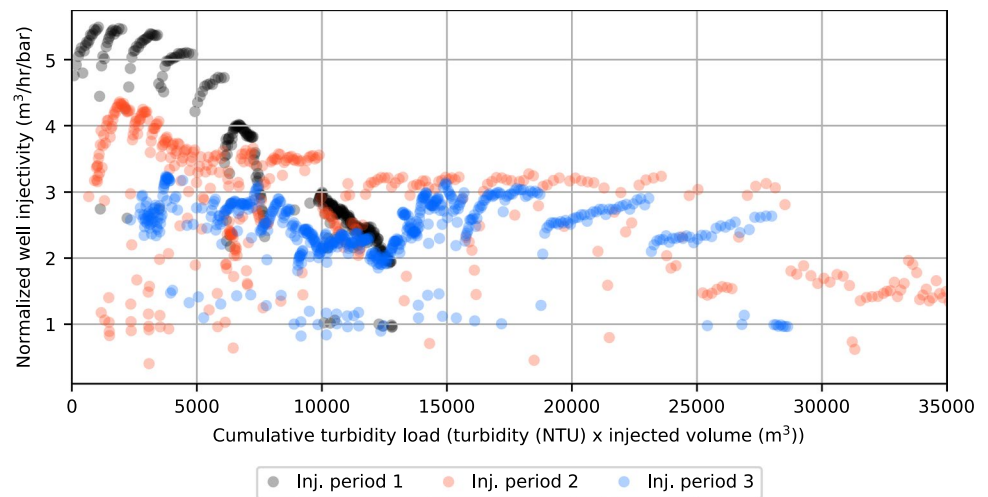


**Fig. 7** Overview of the normalized well injectivity versus the cumulative turbidity load—turbidity (NTU) × injected volume ( $\text{m}^3$ )—during the three injection periods



### Feasibility of ASTR with tile drainage water

The timespan of this study on clogging was relatively short (~1.5 years) compared to the lifetime of an ASTR system (several decades). Injecting larger volumes over longer periods of time may result in clogging due to mechanisms unnoticed in the current study. This study showed that TDW turbidity can largely vary over time and relates to rainfall events. Disc filters were not sufficient to prevent clogging, as highly turbid TDW resulted in rapid clogging of the well screen, borehole wall, aquifer, and/or disc filters. Well clogging substantially decreased after adding automated periodic backflushing of the injection wells and regulating the maximum turbidity (<20 NTU). It also resulted in a loss of injected TDW volume of ~10% by backflushing ( $5 \text{ m}^3$  after  $50 \text{ m}^3$  injection) and another ~10–15% as a consequence of the turbidity regulation. Altogether this represents a loss of injected TDW of 20–25%. Reducing the maximum turbidity to <5 NTU as proposed by Martin (2013) would certainly further decrease the degree of well clogging, but would at this site lead to a dramatic reduction of 80–85% of TDW that is available for injection. This is a major disadvantage of the proposed clogging-prevention measures. Agricultural ASTR is, therefore, only practically and economically attractive using these measures, if a large enough volume of water can be injected that can secure the farmers' need for fresh irrigation water. Soil composition and tile drainage system design that would lead to TDW with a considerably lower turbidity would make the business case more favorable. An alternative for regulating maximum turbidity would be to further treat TDW, although treatment is often restricted by financial, spatial, or practical limitations.

### Conclusion

The current study analyzed well clogging of an aquifer storage transfer and recovery (ASTR) system in which tile drainage water (TDW) was collected from an agricultural parcel (10 ha), stored in an aquifer, and later abstracted and reused for irrigation. This system was susceptible to well clogging, as TDW composition considerably surpassed most clogging mitigation guidelines (e.g., mean injected DOC: 25 mg/L,  $\text{NO}_3^-$ : 14 mg/L, turbidity: 2–165 NTU). Increasing turbidity values related to large rainfall events, during which precipitates and microbial deposits were released from the drain interiors due to the higher water pressures and flow velocities. Slow and rapid sand filtration successfully prevented well clogging of a smaller-scale (2.3 ha) ASR pilot which was previously studied at the same farm. These clogging-prevention measures occupy a large area above ground and have relatively high costs. Therefore, three alternative measures were studied in three injection periods over 1.5 year of ASTR operation. Injected tile drainage water (TDW) was treated with 40- $\mu\text{m}$  disc filters in the first injection period. Nonetheless, the normalized well injectivity decreased quickly over time and video footage showed a substantially clogged well screen. Clogging was associated with physical, chemical, and biological processes, based on the results of elemental, organic carbon, 16S rRNA, and grain-size analysis. The injected turbidity load is strongly related to the decrease in normalized well injectivity, which suggests that particles in injected TDW were the prime source of clogging. Rehabilitation did not fully recover the well to the initial injectivity, which suggests that also the borehole wall and aquifer were clogged. In the second injection period,

automated periodic backflushing of the injection wells was added as a clogging-prevention measure, which resulted in less clogging. However, a severe rainfall event (44 mm in 3 days) resulted in discharge of highly turbid TDW (up to 165 NTU) which rapidly clogged the disc filters. In the last injection period, the turbidity of TDW was regulated (<20 NTU), in addition to the previous measures. The ASTR operation was preserved, but the injected TDW volume decreased by ~20–25% due to the backflushing and turbidity regulation. The three measures together not only reduced clogging substantially, but also significantly reduced the volume of water available for injection. Agricultural ASTR is therefore only feasible by using the studied clogging-prevention measures, but also important is whether or not the injected water volume adequately secures the freshwater needs of the farmer.

**Supplementary Information** The online version contains supplementary material available at <https://doi.org/10.1007/s10040-023-02602-z>.

**Acknowledgements** Firstly, we would like to highlight that as Julian Ros and Emiel Kruisdijk contributed equally do this work, both deserved to be the first author of this paper. Secondly, we would like to thank Vita Marquenie for her contribution to the fieldwork and 16S rRNA analysis. Patricia van den Bos, Jane Erkemeij, and Armand Middeldorp at the Department of Sanitary Engineering of the Delft University of Technology are acknowledged for their assistance during sample preparation and analysis.

**Funding** This research has been financially supported by the Netherlands Organization for Scientific Research (NWO; Topsector Water Call 2016; project acronym AGRIMAR; contract number: ALWTW.2016.023) with co-funding from private partners Acacia Water B.V., Broere Beregening B.V., and Delphy B.V.

## Declarations

**Conflict of interest** The authors declare that they have no conflict of interest.

**Open Access** This article is licensed under a Creative Commons Attribution 4.0 International License, which permits use, sharing, adaptation, distribution and reproduction in any medium or format, as long as you give appropriate credit to the original author(s) and the source, provide a link to the Creative Commons licence, and indicate if changes were made. The images or other third party material in this article are included in the article's Creative Commons licence, unless indicated otherwise in a credit line to the material. If material is not included in the article's Creative Commons licence and your intended use is not permitted by statutory regulation or exceeds the permitted use, you will need to obtain permission directly from the copyright holder. To view a copy of this licence, visit <http://creativecommons.org/licenses/by/4.0/>.

## References

Andrews S (2010) Babraham bioinformatics-FastQC: a quality control tool for high throughput sequence data. <https://www.bioinformatics.babraham.ac.uk/projects/fastqc>. Accessed Jan 2022

- Abbott CL, Leeds-Harrison PB (1998) Research priorities for agricultural drainage in developing countries. HR Wallingford, Firm
- Bayer B, Saito MA, McIlvin MR, Lückler S, Moran DM, Lankiewicz TS, Dupont CL, Santoro AE (2021) Metabolic versatility of the nitrite-oxidizing bacterium *Nitrospira marina* and its proteomic response to oxygen-limited conditions. *ISME J* 15:1025–1039
- Brehme M, Regenspurg S, Leary P, Bulut F, Milsch H, Petrauskas S, Valickas R, Blöcher G (2018) Injection-triggered occlusion of flow pathways in geothermal operations. *Geofluids* 2018:4694829
- Camprovin P, Hernández M, Fernández S, Martín-Alonso J, Galofré B, Mesa J (2017) Evaluation of clogging during sand-filtered surface water injection for aquifer storage and recovery (ASR): pilot experiment in the Llobregat Delta (Barcelona, Spain). *Water* 9:263
- Caporaso JG, Kuczynski J, Stombaugh J, Bittinger K, Bushman FD, Costello EK, Fierer N, Peña AG, Goodrich JK, Gordon JI, Huttenley GA, Kelley ST, Knights D, Koenig JE, Ley RE, Lozupone CA, McDonald D, Muegge BD, Pirrung M et al (2010) QIIME allows analysis of high-throughput community sequencing data. *Nat Methods* 7:335–336
- Daebeler A, Bodelier PLE, Yan Z, Hefting MM, Jia Z, Laanbroek HJ (2014) Interactions between Thaumarchaea, *Nitrospira* and methanotrophs modulate autotrophic nitrification in volcanic grassland soil. *ISME J* 8:2397–2410
- Delft University of Technology (2022) ASTR injection well clogging. Accession PRJNA809926, hosted on the National Library of Medicine. <https://www.ncbi.nlm.nih.gov/bioproject/809926>. Accessed 18 Jan 2023
- Dillon PJ, Hickinbotham MR, Pavelic P (1994) Review of international experience in injecting water into aquifers for storage and reuse. In *Water Down Under 94: Groundwater Papers; Preprints of Papers: Groundwater Papers; Preprints of Papers*. Institution of Engineers, Barton, ACT, pp 13–14
- Dillon P (2005) Future management of aquifer recharge. *Hydrogeol J* 13:313–316
- Dillon P, Stuyfzand P, Grischek T, Lloria M, Pyne R, Jain R, Bear J, Schwarz J, Wang W, Fernandez E (2019) Sixty years of global progress in managed aquifer recharge. *Hydrogeol J* 27:1–30
- Emerson D, De Vet W (2015) The role of FeOB in engineered water ecosystems: a review. *J AWWA* 107:E47–E57
- Eom H, Flimban S, Gurung A, Suk H, Kim Y, Kim YS, Jung SP, Oh S-E (2020) Impact of carbon and nitrogen on bioclogging in a sand grain managed aquifer recharge (MAR). *Environ Eng Res* 25:841–846
- Glodowska M, Stopelli E, Schneider M, Rathi B, Straub D, Lightfoot A, Kipfer R, Berg M, Jetten M, Kleindienst S, Kappler A, Glodowska M, Kappler A, Kleindienst S, Cirpka OA, Rathi B, Lightfoot A, Stopelli E, Berg M, et al. (2020) Arsenic mobilization by anaerobic iron-dependent methane oxidation. *Commun Earth Environ* 1:42
- Greve P, Kahil T, Mochizuki J, Schinko T, Satoh Y, Burek P, Fischer G, Tramberend S, Burtscher R, Langan S, Wada Y (2018) Global assessment of water challenges under uncertainty in water scarcity projections. *Nat Sustain* 1:486–494
- Hubbs SA (2006) *Riverbank filtration hydrology*. Taylor and Francis, Dordrecht, The Netherlands
- Jeong HY, Jun S-C, Cheon J-Y, Park M (2018) A review on clogging mechanisms and managements in aquifer storage and recovery (ASR) applications. *Geosci J* 22:667–679
- Jorgensen BB (1989) Biogeochemistry of chemoautotrophic bacteria. In: *Autotrophic bacteria*. Science Tech, Madison, WI, pp 117–146
- Knudson M (1901) *Hydrographical tables*. GEC Gad, Copenhagen, 63 pp
- Krepeski ST, Hanson TE, Chan CS (2012) Isolation and characterization of a novel biomineral stalk-forming iron-oxidizing bacterium

- from a circumneutral groundwater seep. *Environ Microbiol* 14:1671–1680
- Maliva RG (2020) Anthropogenic aquifer recharge and water quality. In: *Anthropogenic aquifer recharge*. Springer, Dordrecht, The Netherlands, pp 133–164
- Martin R (2013) Clogging issues associated with managed aquifer recharge methods. IAH Commission on Managing Aquifer Recharge. [https://recharge.iah.org/files/2015/03/Clogging\\_Monograph.pdf](https://recharge.iah.org/files/2015/03/Clogging_Monograph.pdf). Accessed Jun 2021
- Mayer TD, Jarrell WM (2000) Phosphorus sorption during iron(II) oxidation in the presence of dissolved silica. *Water Res* 34:3949–3956
- Muyzer G, Waal ECD, Uitterlinden AG (1993) Profiling of complex microbial populations by denaturing gradient gel electrophoresis analysis of polymerase chain reaction-amplified genes coding for 16S rRNA. *Appl Environ Microbiol* 59:695–700
- Okubo T, Matsumoto J (1983) Biological clogging of sand and changes of organic constituents during artificial recharge. *Water Res* 17:813–821
- Olsthoorn T (1982) The clogging of recharge wells, main subjects. Keuringsinstituut voor Waterleiding Artikelen, KIWA NV, Rijswijk, The Netherlands
- Page D, Miotliński K, Dillon P, Taylor R, Wakelin S, Levett K, Barry K, Pavelic P (2011) Water quality requirements for sustaining aquifer storage and recovery operations in a low permeability fractured rock aquifer. *J Environ Manag* 92:2410–2418
- Page D, Bekele E, Vanderzalm J, Sidhu J (2018) Managed aquifer recharge (MAR) in sustainable urban water management. *Water* 10:239
- Parkhurst DL, Appelo CAJ (2013) Description of input and examples for PHREEQC version 3: a computer program for speciation, batch-reaction, one-dimensional transport, and inverse geochemical calculations. US Geological Survey Techniques and Methods, USGS, Reston, VA, 519 pp
- Pavelis GA (ed) (1987) *Farm drainage in the United States: History, status, and prospects* (No. 1455). US Department of Agriculture, Economic Research Service
- Pyne RDG (1995) *Groundwater recharge and wells: a guide to aquifer storage recovery*. Routledge, New York
- Reiche M, Torburg G, Küsel K (2008) Competition of Fe(III) reduction and methanogenesis in an acidic fen. *FEMS Microbiol Ecol* 65:88–101
- Rinck-Pfeiffer S, Ragusa S, Sztajn bok P, Vandeveld T (2000) Interrelationships between biological, chemical, and physical processes as an analog to clogging in aquifer storage and recovery (ASR) wells. *Water Res* 34:2110–2118
- Rivera M (2017) Bacterioferritin: structure, dynamics, and protein–protein interactions at play in iron storage and mobilization. *Acc Chem Res* 50:331–340
- Schneider K, Rose I, Vikineswary S, Jones AL, Goodfellow M, Nicholson G, Beil W, Süßmuth RD, Fiedler H-P (2007) Nocardichelins A and B, Siderophores from *Nocardia* strain Acta 3026. *J Nat Prod* 70:932–935
- Smedema LK, Ochs WJ (1997) *The state of land drainage in the world*. International Commission on Irrigation and Drainage, New Delhi
- Stikker A (1998) Water today and tomorrow: prospects for overcoming scarcity. *Futures* 30:43–62
- Stoecker K, Bendinger B, Schöning B, Nielsen PH, Nielsen JL, Baranyi C, Toenshoff ER, Daims H, Wagner M (2006) Cohn's Crenothrix is a filamentous methane oxidizer with an unusual methane monooxygenase. *Proc Natl Acad Sci* 103:2363–2367
- Stuyfzand PJ (1993) *Hydrochemistry and hydrology of the coastal dune area of the Western Netherlands*. PhD Thesis, Vrije University, Amsterdam, The Netherlands
- Stuyfzand PJ, Osma J (2019) Clogging issues with aquifer storage and recovery of reclaimed water in the brackish Werribee aquifer, Melbourne, Australia. *Water* 11:1807
- Stuyfzand PJ, Osma J (2020) Water quality aspects and clogging of the West Werribee ASR operational trial, Melbourne (Australia). Technical Report No. KWR 2018.071, KWR, Nieuwegein, The Netherlands, 90 pp
- Stuyfzand PJ, Juhász-Holterman MHA, de Lange WJ (2006) Riverbank filtration in the Netherlands: well fields, clogging and geochemical reactions. In: Hubbs SA (ed) *Riverbank filtration hydrology*. Springer, Netherlands, pp 119–153
- Süsser P, Schwertmann U (1983) Iron oxide mineralogy of ochreous deposits in drain pipes and ditches. *Kulturtechn Flurber* 24:386–395
- Tamura K, Stecher G, Kumar S (2021) MEGA11: molecular evolutionary genetics analysis version 11. *Mol Biol Evol* 38:3022–3027
- TNO-NITG, TNO-NITG DINOloket (2021) GeoTop model. <http://www.dinoloket.nl>. Accessed May 2022
- Tolk L, Veldstra J (2016) Spaarwater, pilots rendabel en duurzaam agrarisch watergebruik in een verziltende omgeving van de waddenregio [Saving water, pilots on profitable and sustainable agricultural water use in a salinizing environment of the Wadden region]. Main report, Acacia Institute, East Perth, Australia
- Tuomanen EI, Sokol PA, Darling P, Lewenza S, Corbett CR, Kooi CD (2000) Identification of a Siderophore receptor required for ferric Ornibactin uptake in *Burkholderia cepacia*. *Infect Immun* 68:6554–6560
- Vanderzalm JL, La Salle CLG, Dillon PJ (2006) Fate of organic matter during aquifer storage and recovery (ASR) of reclaimed water in a carbonate aquifer. *Appl Geochem* 21:1204–1215
- Walter F (1976) *Geophysical well logging for geohydrological purposes in unconsolidated formations*. Dienst Grondwaterverkenning TNO, Delft, The Netherlands
- Zuurbier KG, van Dooren T (2019) Urban waterbuffer Spangen: resultaten [Urban water buffer Spangen: results]. KWR. <http://api.kwrwater.nl/uploads/2020/01/KWR-2019.111-Urban-Water-buffer-Spangen-Resultaten.-Deelrapport-TKI-project-Urban-Waterbuffer.pdf>. Accessed Jun 2021
- Zuurbier KG, Zaadnoordijk WJ, Stuyfzand PJ (2014) How multiple partially penetrating wells improve the freshwater recovery of coastal aquifer storage and recovery (ASR) systems: a field and modeling study. *J Hydrol* 509:430–441

**Publisher's note** Springer Nature remains neutral with regard to jurisdictional claims in published maps and institutional affiliations.